Laser-induced fluorescence measurements of resonance broadening in xenon

R. J. Cedolin, R. K. Hanson, and M. A. Cappelli
High Temperature Gasdynamics Laboratory, Stanford University, Stanford, California 94305-3032
(Received 16 October 1995; revised manuscript received 15 December 1995)

Resonance broadening in atomic xenon has been studied by using laser-induced fluorescence of two excited-state electronic transitions. The impact theory result for resonance broadening is verified to be accurate and the onset of the breakdown of the theory is chronicled. The spectral broadening of the $6s[3/2]_1^o(^3P_1)\rightarrow 6p[1/2]_0$ (828-nm) transition by the resonant interaction of its lower level with ground-state xenon was investigated for densities of 4×10^{21}–2×10^{24} atoms m^{-3}. The predominantly Doppler-broadened $6s[3/2]_2^o(^3P_2)\rightarrow 6p[3/2]_2$ (823-nm) transition was analyzed for similar conditions, primarily to establish the kinetic temperature of the neutral xenon. Tunable narrow-linewidth semiconductor diode lasers were used to probe the excited states, which were produced by a direct-current glow discharge. The intricate hyperfine structure of the measured profiles was taken into account by summing constituent Voigt profiles to construct model line shapes. The $6s[3/2]_1^o\rightarrow 6p[1/2]_0$ broadening constant at low densities and at 311 K was found to be $6.04(\pm0.66)\times10^{-21}$ MHz m^3 $atom^{-1}$. This result is in agreement with the value predicted by the impact theory for resonance broadening. The $6s[3/2]_1^o\rightarrow 6p[1/2]_0$ Lorentzian width extrapolated to zero density, 43 ± 15 MHz, is in accord with the natural linewidth. At densities above 6×10^{23} atoms m^{-3} the recorded line shapes of this transition exhibited an asymmetry, providing clear evidence of the breakdown of the impact approximation. The measured Lorentzian broadening for the $6s[3/2]_2^o\rightarrow 6p[3/2]_2$ transition was $8.3(\pm1.8)\times10^{-22}$ MHz m^3 $atom^{-1}$ at 311 K. [S1050-2947(96)01807-0]

PACS number(s): 32.70.Jz, 32.10.Fn, 32.70.Cs

I. INTRODUCTION

The use of spectroscopic line-shape analysis for the determination of parameters of the environment of an atom or molecule is a common and valuable diagnostic technique. This technique is critically dependent on the accuracy and validity of the prevailing theoretical understanding of the physical processes involved in spectral line broadening. The strong resonant transitions of the noble gases allow for the study of pure resonance broadening, uncomplicated by nonresonant collisional interactions. As the resonant transitions are deep in the ultraviolet and are subject to considerable radiative trapping, experimental work has focused on spectral lines with the resonance level as the lower level [1–13]. These previous studies have concentrated on the lighter inert gases.

We present here an investigation into the resonance broadening of xenon using analyses of the spectral line shapes of two excited-state transitions. As shown in Fig. 1, xenon's $6s[3/2]_1^o(^3P_1)$ level is resonantly coupled to the ground state. The $^3P_1$ level appears as a second resonance level in the inert gases as Russell-Saunders coupling breaks down at the higher atomic numbers. For xenon, as opposed to the lighter inerts, the $^1S_0\rightarrow{}^3P_1$ transition is slightly stronger than the $^1S_0\rightarrow{}^1P_1(6s'[1/2]_1^o)$ line [14]. Thus resonance broadening is an important broadening mechanism for the $6s[3/2]_1^o\rightarrow 6p[1/2]_0$ transition. In contrast, the $6s[3/2]_2^o\rightarrow 6p[3/2]_2$ transition is broadened mainly by the Doppler effect as the $6s[3/2]_2^o(^3P_2)$ level is metastable. In a demonstration of the capabilities of diode lasers, Pine, Glassbrenner, and Kafalas [15] recorded absorption line shapes of these severely hyperfine-split transitions. A combination of isotopic and nuclear-spin splitting makes these line shapes a complex conglomeration of individual lines. Stacey and Thompson [1] have shown with neon that the resonance broadening interaction between unlike isotopes is commensurate with that between identical ones. Also, the effect of the nuclear spin of the odd isotopes is predicted to not be significant if the collisions are diabatic with respect to the nuclear spin splitting (i.e., the inverse of the collision duration must be much larger than the hyperfine splitting) [16,17]. Calculations show that the diabatic assumption is reasonable for the transitions of interest. These considerations, combined with a complete understanding of the un-

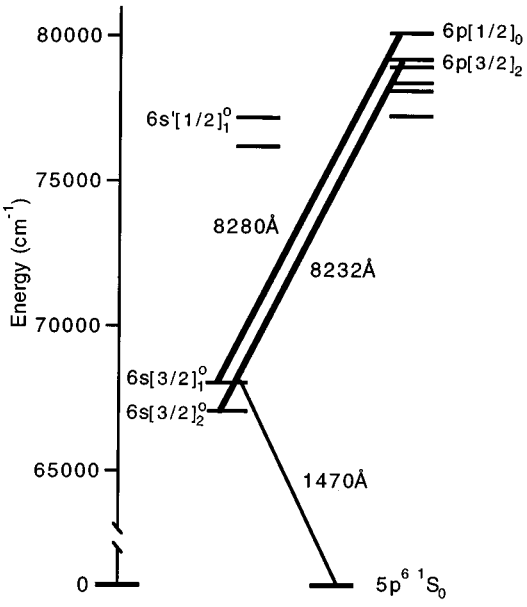

FIG. 1. Partial energy-level diagram of xenon. Energy-level values are from [47].

derlying hyperfine structure, have permitted our investigation into the line broadening.

Theoretical calculations for resonance broadening in the impact regime produce a simple result for the resonance full width at half maximum (FWHM) [18]:

$$\Delta\nu_{\rm res}=\frac{cr_e}{8}k_{jj'}f_{\rm res}\lambda_{\rm res}N. \quad (1)$$

Here the classical electron radius is represented by r_e, c is the speed of light, $\lambda_{\rm res}$ is the wavelength of the resonant transition, and $k_{jj'}$ is a constant determined by the quantum numbers j and j' of the ground and resonance levels. For all noble gases, $j=0$ and $j'=1$. The theoretical value for this case is $k_{01}=1.53$ [17,19]. The FWHM is predicted to be temperature independent and to have a linear dependence on the species number density N and on the resonant oscillator strength $f_{\rm res}$.

Other Lorentzian broadening mechanisms of $6s[3/2]_1^o\rightarrow 6p[1/2]_0$ are not significant for the conditions of interest. The dispersion or van der Waals contribution to the broadening can be safely neglected for strong resonant transitions. Lewis [20] has shown that the dispersion contribution does not simply add to the resonance broadening. For a resonant component more than three times as great as what the dispersion component would be if acting alone, the dispersion contribution to the line shape is entirely negligible. The van der Waals interaction is of the same order across transitions between the same manifolds of fine-structure levels [21]. So the magnitude of the van der Waals broadening of the $6s[3/2]_2^o\rightarrow 6p[3/2]_2$ transition can serve as a check on the assumption to neglect the dispersion contribution to the $6s[3/2]_1^o\rightarrow 6p[1/2]_0$ line shape. Stark broadening data is unavailable for these transitions. It is estimated to be negligible from rough calculations [22] and from extrapolation of data from other noble-gas species [23].

Emission studies of resonance broadening have been complicated by non-Gaussian velocity distributions of highly excited states in the direct-current (dc) discharge plasmas employed [1–7]. One result of this difficulty was the disagreement of the Lorentzian width extrapolated to zero density with the natural linewidth. This ''extrapolation anomaly'' has recently been investigated in detail for neon [24].

Absorption studies of the resonance broadening have proven more reliable. First, they sidestep the problem of incomplete thermalization of the higher-lying levels. Emission line shapes are affected by the velocity distribution in the upper, emitting, state, whereas absorption probes the lower, resonance, level. Higher-lying states are more likely to be formed by dissociative recombination of molecular ions with electrons, which gives rise to neutral atoms with excess kinetic energy. As a result, these states are not thermalized at the gas kinetic temperature. Lower-lying states are predominantly populated by electron-impact excitation and radiative cascade [24]. These levels are then better thermalized into a velocity distribution closer to a Gaussian. The second advantage of absorption studies is that the use of a narrow-linewidth laser can reduce the complications of the instrumental contribution to the line shape. Using helium [8] and neon [9,10], laser absorption experiments have been used to verify the resonance broadening theory [Eq. (1)]. However, little work has been done with the heavier inert gases.

The technique we use in this study, laser-induced fluorescence (LIF), effectively measures the absorption line shape by monitoring the fluorescence from a small region following absorption of the probe laser beam. To our knowledge, our measurements are the first test of the low-density resonance broadening theory for xenon and are the first to extend the measurements of absorption line shapes in helium and neon [8,9] to heavier inert gases. Furthermore, Lindsay, Nicol, and Stacey [9] detect a nonlinearity in the dependence of the FWHM on the number density at the high-number-density end of their data set. They suggest that it may be caused by the onset of the breakdown of the impact approximation. An earlier emission study of krypton showed a similar indication [2]. A nonlinearity in the FWHM versus number density for the resonance broadening of an excited level is predicted by Srivastava and Zaidi [25] in the transition from the impact to the static limit. Vaughan could not detect asymmetries at the high densities where a nonlinearity in krypton was observed [2]. In our investigation, measurements were extended to high enough densities to allow for the observation of statistical collision behavior in the form of asymmetric line shapes. As reviewed in Refs. [26] and [27], asymmetric line shapes signal a departure from the impact limit.

This study also demonstrates how knowledge of the underlying hyperfine structure and an understanding of the appropriate broadening mechanisms can enable the use of spectral-line shapes as a diagnostic tool in xenon plasmas. As a rare gas with low ionization potential and high molecular weight, xenon is being used extensively as a propellant in the study of ion thrusters [28] and Hall thrusters [29] for satellite propulsion. Single-point LIF has been shown in studies of electrothermal hydrogen arc-jet thrusters to be a valuable diagnostic tool by offering measurement capabilities of kinetic temperatures and atomic velocities for comparison to physical models [30]. LIF provides the high spatial resolution essential in probing the nonuniform plasma environments encountered in electric propulsion devices. An extension of the LIF line-shape analysis to xenon transitions should prove to be as valuable in the study of xenon plasma thrusters.

II. EXPERIMENT

The plasma source for excited xenon atoms was a room-temperature hollow-cathode dc discharge. The xenon (SpectraGases 99.999% pure) was metered at 0.5 to 1 SCCM, where SCCM denotes cubic centimeter per minute at STP, through the discharge tube, which had a 1-cm-square cross section. The pressure was measured just downstream of the discharge by capacitance manometers (MKS Baratron, 0–10 and 0–100 torr) of 0.5% accuracy. A mechanical pump reduced the system pressure to 10 mtorr and the system was flushed with xenon a few times before the experiment was performed. Line shapes were measured for pressures from 0.13 to 52 torr. For each line-shape measurement, the pressure was recorded and verified to have remained within $\pm 1\%$ of the nominal pressure throughout. A thermocouple bead of 0.6 mm diameter was positioned against the glass to monitor the temperature on the outer wall of the discharge. A nomi-

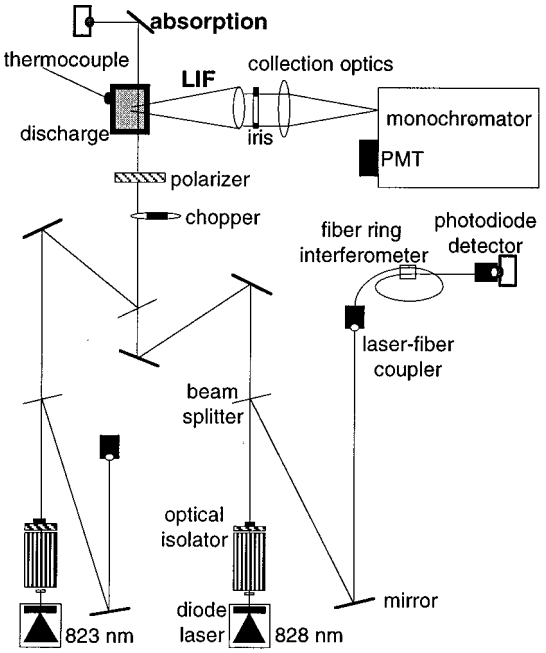

FIG. 2. Experimental setup.

nal discharge current of 0.36 mA was used at densities below 3×10^{23} atoms m^{-3}. The discharge could not be sustained with this current at higher densities so 1 mA was used for the remaining measurements. A sample measurement at 9×10^{22} atoms m^{-3} was taken with a discharge current of 1 mA and it was found to be consistent with the low-density 0.36-mA results. Other research has also demonstrated an insensitivity of the results to the discharge current [3,4,8]. This insensitivity lends credence to our assumption of the insignificance of Stark broadening.

A schematic of the experiment is shown in Fig. 2. The light sources were AlGaAs semiconductor diode lasers, which have Lorentzian emission profiles with a typical linewidth of 10 MHz [31]. The lasers were tuned by current modulation. Both beams first passed through optical isolators to prevent backreflections from affecting laser operation. A portion of each beam was then split off to enable the frequency to be monitored. The monitoring was performed by a fiber ring interferometer [32]. This interferometer was calibrated with a 2-GHz solid confocal étalon and found to have a free spectral range of 178.4 ± 0.4 MHz. The remainder of each beam was joined onto a coincident path through the discharge.

The beam entering the discharge was mechanically chopped at 1 kHz to allow for phase-sensitive detection. A motorized rotating polarizer was used to keep the intensity far below the saturation intensity appropriate to the specific transition and discharge conditions. The saturation intensities were found experimentally to be about 0.2 mW mm^{-2} for the 823-nm transition and about 3 mW mm^{-2} for the 828-nm transition at 1 torr. To avoid complications from power broadening of the line shape, the laser intensity was kept at a level calculated to give only about a 1% reduction in the peak absorption from saturation.

The 5×2 mm^2 laser beam entered the discharge near the LIF collection side to minimize radiative trapping, with the 5-mm side parallel to the collection side of the discharge. A silicon photodiode monitored the beam intensity that passed through the discharge, providing a measure of the absorption. The spectrally resolved fluorescence was collected at right angles to the incident beam. A half-meter monochromator was used as a spectral filter, passing light over the entire transition while the laser frequency was varied. The LIF was detected by a photomultiplier tube. Lock-in amplifiers were used for both the LIF and absorption signals. LIF excitation scans using the 823- and 828-nm lasers were taken consecutively with the discharge continually operating at the same conditions. Each single trace recorded took from 10 to 240 s depending on the LIF signal strength at the given conditions. Multiple traces were recorded and separately analyzed at each pressure.

III. ANALYSIS

The line shapes for each of the two transitions investigated are composed of a number of hyperfine lines. Xenon has nine stable isotopes, three with natural abundances greater than 20% (^{132}Xe,^{131}Xe,^{129}Xe) [33]. The isotopic shifts required to construct model line shapes were taken from measurements in Refs. [34] and [35]. The isotopes ^{131}Xe and ^{129}Xe with odd atomic mass number have nonzero nuclear-spin angular momenta, which give rise to further hyperfine splitting. The nuclear-spin shifts from the origins of the hyperfine multiplets (given by the isotopic shift) were calculated using parameters that have been measured for each of the levels involved in the relevant transitions [36,37]. The isotopic abundance ratios were used for the relative intensities of the separate isotopic lines (summed over hyperfine components). Any effect discharge mechanisms could have on the relative density distributions of the isotopes was assumed to be small because of the small mass differences between the predominant isotopes. For the isotopes possessing a nuclear magnetic moment, the intensity was distributed between the hyperfine components according to quantum-mechanical sum rules [38]. The positions and relative intensities of the 21 hyperfine components contributing to the $6s[3/2]^o_2\rightarrow6p[3/2]_2$ line shape are shown within a sample LIF trace in Fig. 3. The $6s[3/2]^o_1\rightarrow6p[1/2]_0$ transition is composed of 12 hyperfine components. Each hyperfine component was individually broadened into a Voigt profile. Atomic velocity correlation effects were estimated to be negligible [39] so the contributing hyperfine line shapes could be accurately represented by Voigt profiles, which convolve Gaussian (Doppler) and Lorentzian contributions. The relative broadening of the hyperfine-split lines was fixed according to the relative masses of the isotopes. The resulting intensities were added to construct an excitation spectrum to model the reduced recorded line shapes.

The recorded absorption trace was used to calculate the intensity incident on the LIF collection volume to normalize the LIF data. The absorption never exceeded 1% for the $6s[3/2]^o_1\rightarrow6p[1/2]_0$ transition and was less than 8% for $6s[3/2]^o_2\rightarrow6p[3/2]_2$. The recorded interferometer data were then used to transform the LIF data into frequency space to give the reduced line shape.

No correction was made to the LIF spectra to account for the approximately 10-MHz Lorentzian linewidth of the diode lasers. As it contributed an equal amount to each detected

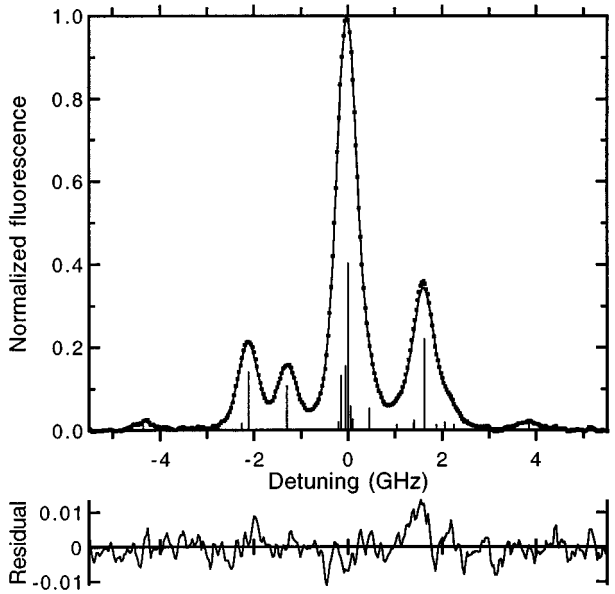

FIG. 3. $6s[3/2]_2^o \rightarrow 6p[3/2]_2$ line shape: •, reduced LIF excitation data with only every fifth point plotted for clarity and Voigt $a=0.33$; |, hyperfine lines contributing to the line shape; —, curve fit result from sum of Voigt broadened hyperfine lines with residual.

LIF line shape, the slope of a plot of the Lorentzian broadening versus number density would not be affected by it. The laser linewidth would influence only the intercept of the data. Furthermore, if the laser emission profile had any Gaussian component it would have had a negligible affect on the Doppler FWHM of the recorded LIF line shape. As Gaussian components add according to their squares, even a fully Gaussian laser linewidth of 10 MHz would have had a small effect when convolved with the 400-MHz Doppler broadening of the xenon transitions at room temperature.

The reduced LIF line shape was introduced to a χ^2-minimization curve-fitting procedure that optimized the kinetic temperature T_{kin} (which determined the Doppler FWHM) and the Lorentzian FWHM $\Delta\nu_L$ to most closely match the data. This Lorentzian FWHM should be almost entirely composed of the $\Delta\nu_{\text{res}}$ of Eq. (1) for the $6s[3/2]_1^o \rightarrow 6p[1/2]_0$ transition. The line positions and relative intensities were fixed in the fitting procedure. The overall amplitude, a linear base line, T_{kin}, and $\Delta\nu_L$ were the parameters to the fit. Figure 3 shows a reduced $6s[3/2]_2^o \rightarrow 6p[3/2]_2$ line shape with the corresponding curve-fit result overlaid onto the data and the fit residual displayed below it. This line shape was mainly Doppler broadened as indicated by the Voigt a parameter value of 0.33. The ability to accurately fit the reduced line shape demonstrates that the hyperfine-splitting data from the literature has proven to be of adequate accuracy for this study. A fit residual within 1–2 % of the peak height was representative of all analyzed line shapes. For the $6s[3/2]_1^o \rightarrow 6p[1/2]_0$ transition, T_{kin} was fixed to the value measured from the $6s[3/2]_2^o \rightarrow 6p[3/2]_2$ line shapes to allow the fit to more accurately find $\Delta\nu_L$.

An alternate analysis procedure involved removal of the background from the data before the curve-fitting procedure. The background was then no longer a parameter to the fit. The signal background was composed of laser reflections from the discharge glass and discharge emission that corresponded in frequency to the lock-in amplifier detection bandwidth. The background signal was recorded before and after each LIF measurement. Thirteen representative line shapes for each transition underwent both analysis methods. There were no significant differences in the results.

IV. RESULTS

The kinetic temperature measured from the Doppler widths of the $6s[3/2]_2^o \rightarrow 6p[3/2]_2$ transition was used to convert the measured discharge pressures to number densities. Thirteen $6s[3/2]_2^o \rightarrow 6p[3/2]_2$ line shapes were recorded and analyzed at six different discharge conditions. The Voigt a parameters of these line shapes varied from 0.02 to 0.36. The kinetic temperatures measured in this way showed no systematic dependence on the discharge operating conditions. Once the lack of pressure dependence was established, $6s[3/2]_2^o \rightarrow 6p[3/2]_2$ line shapes were no longer recorded and the average of T_{kin} over all measurements was used. The 311 ± 33 K average was slightly higher than the discharge wall temperature of around 300 K. Because of the low discharge current used, the thermocouple measurement of the outer discharge wall was unchanged from the ambient room temperature by discharge operation.

Kinetic temperatures were also derived from the Doppler width of the $6s[3/2]_1^o \rightarrow 6p[1/2]_0$ line shapes. At densities below 10^{23} atoms m^{-3} (Voigt $a<1.4$), these measurements were consistent with the 311 K average of the $6s[3/2]_2^o \rightarrow 6p[3/2]_2$ measurements. Above this density though, the increased Lorentzian component made the $6s[3/2]_1^o \rightarrow 6p[1/2]_0$ line shape less sensitive to the Doppler width and the derived temperatures became more erratic.

Figure 4 displays reduced $6s[3/2]_1^o \rightarrow 6p[1/2]_0$ LIF spectra demonstrating the evolution of the resonance-broadened line shape with increasing pressure. The corresponding curve-fit results are included. The lowest-density measurement is shown in Fig. 4(a). The discharge could not be sustained at substantially lower densities and the Doppler broadening, which was constant over all densities, was becoming predominant. The 12 hyperfine components are shown within the line shape in Fig. 4(a). This transition's hyperfine splitting was only beginning to be resolved at this density. Thirty-five of these line shapes were recorded at seventeen operating conditions.

The resulting Lorentzian FWHM's are plotted against number density in Fig. 5. The theoretical predictions of the resonance broadening from Eq. (1) using previous measurements of f_{res} are displayed with the data over a reduced density range. The full density range is shown in the inset. The error bars on the data display the uncertainty in the number density arising from the uncertainty in the measured neutral kinetic temperature. The low-density end of the error bars were derived from the full $+33$ K uncertainty found above. The high-density side was cut off at the measured wall temperature for the specific discharge operating condition: The kinetic temperature of the neutral xenon could not be less than the ambient room temperature. The vertical error bars are less than the size of the markers as the statistical uncertainties from the curve fits were not significant.

As predicted by Eq. (1), the $\Delta\nu_L$ results were linear with

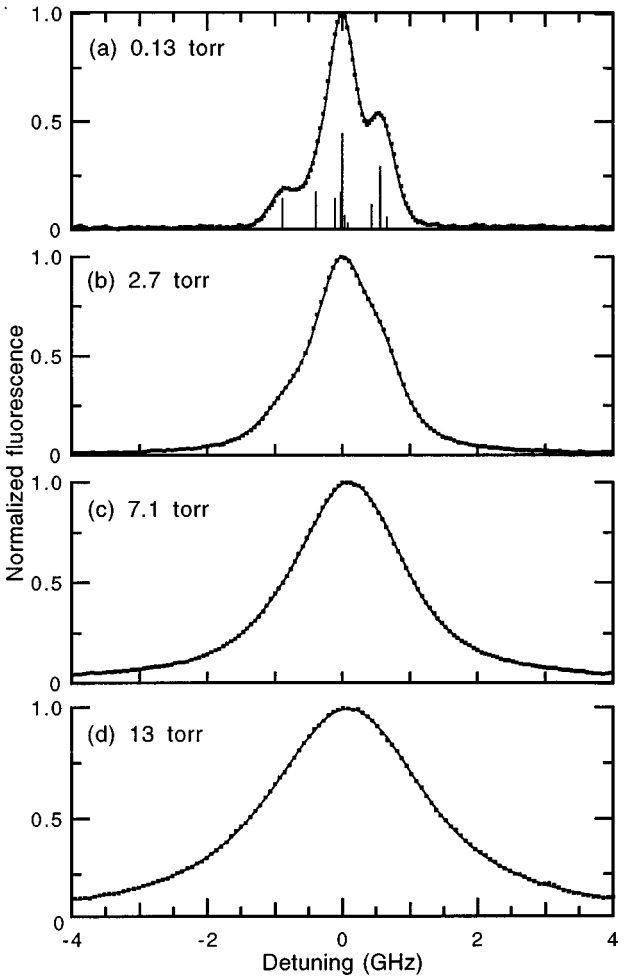

FIG. 4. Evolution of reduced $6s[3/2]_1^o \rightarrow 6p[1/2]_0$ LIF excitation line shapes (•) and curve-fit results (—) with density: (a) 3.9×10^{21} atoms m^{-3} with contributing hyperfine lines (|) with only every sixth point plotted for clarity and Voigt $a=0.16$; (b) 8.4×10^{22} atoms m^{-3} with every tenth point plotted and $a=1.2$; (c) 2.2×10^{23} atoms m^{-3} with every tenth point plotted and $a=2.8$; (d) 4.0×10^{23} atoms m^{-3} with every twenty-fifth point plotted and $a=4.9$.

number density N for low N, as seen in Fig. 5. However, a nonlinearity at higher N is clearly evident in the Fig. 5 inset. To obtain the broadening constant $2\gamma/N$, where γ is the half collision width at half maximum, a line was fit to the linear range of data. Consecutive high-density points were excluded from the fit until an exclusion resulted in less than a 1% change in the slope of the fit. The final result, shown in the Fig. 5 inset, was then based on the 19 measurements below densities of 1.5×10^{23} atoms m^{-3} for which the Voigt a ranged from 0.16 to 2.0. The linear fit result was 6.04×10^{-21} MHz m^3 $atom^{-1}$. The scatter of the data gave a statistical uncertainty (two standard deviations) of 0.01×10^{-21}. Using $T_{\rm kin}=344$ K as the temperature uncertainty limit gave a value 0.65×10^{-21} higher than that using $T_{\rm kin}=311$ K. The total statistical plus experimental uncertainty on $2\gamma/N$ was then 0.66×10^{-21} MHz m^3 $atom^{-1}$. Extrapolating the linear fit to zero density gave 53 MHz with a total uncertainty of 10 MHz arising almost entirely from the uncertainty in the kinetic temperature. This intercept should be composed of the natural linewidth plus the Lorentzian contribution of the laser linewidth. The laser linewidth has not been measured. To be conservative, we allow for a range of ±5 MHz around a nominal laser linewidth of 10 MHz. The result is then 43±15 MHz for the natural linewidth.

The recorded $6s[3/2]_1^o \rightarrow 6p[1/2]_0$ line shapes for densities above 6×10^{23} atoms m^{-3} were not symmetrical. Two such line shapes are presented in Fig. 6. Also displayed on Fig. 6(b) is a line shape constructed of summed Voigt profiles, with their broadening determined by the measured low-density broadening constant for the 2×10^{24} atoms m^{-3} density of the measured spectrum. It is readily apparent that, as well as having a broadening reduced from that of the theory, the profile was no longer of the Voigt shape.

The predominance of Doppler broadening for the $6s[3/2]_2^o \rightarrow 6p[3/2]_2$ transition made the line shape less sensitive to the Lorentzian component. However, sufficient line shapes were recorded to allow for a measure of the broadening constant. Figure 7 shows $\Delta\nu_L$ plotted against N for this transition. The horizontal error bars again reflect the uncertainty in the temperature. The vertical error bars are the statistical uncertainties from the line shape curve fits. The linear fit of the $\Delta\nu_L$ measurements is also displayed. It gave $2\gamma/N=8.3(\pm1.8)\times10^{-22}$ MHz m^3 $atom^{-1}$ with the total uncertainty being evenly split between the statistical uncertainty of the fit and the experimental contribution from the uncertainty of $T_{\rm kin}$. Extrapolation to zero density gave 2.4±11 MHz with the uncertainty being almost entirely statistical.

V. DISCUSSION

The measured broadening constant for $6s[3/2]_1^o \rightarrow 6p[1/2]_0$ can be used to calculate a value for the oscillator strength $f_{\rm res}$ of the resonant transition $5p^6\ {}^1S_0 \rightarrow 6s[3/2]_1^o$. This calculation facilitates a comparison to the theory embodied in Eq. (1). The value $2\gamma/N=6.04(\pm0.66)\times10^{-21}$ MHz m^3 $atom^{-1}$ yields $f_{\rm res}=0.255\pm0.028$. The most recent measurements of this oscillator strength are 0.264±0.016 [40], 0.273±0.014 [14], 0.222±0.027 [41], and 0.260±0.05 [42]. The direct total absorption measurement described in Ref. [40] assumes that Eq. (1) is valid. Recent semiempirical calculations gave 0.223 and 0.208±0.027 with the difference in the results arising from the approximations employed [43]. Calculations of the $6s[3/2]_1^o \rightarrow 6p[1/2]_0$ resonance broadening from Eq. (1) using each of the above previous $f_{\rm res}$ measurements are displayed in Fig. 5 along with the measured Lorentzian FWHM's. The density range is reduced to the linear region with the full density range shown in the inset. Our data lie most closely to the theoretical broadening based on Ferrell, Payne, and Garrett's 0.260 measurement of $f_{\rm res}$ [42]. Although the uncertainty range of the present measurement overlaps that of Suzuki *et al.* [41], the value 0.222 of Suzuki *et al.* is notably lower than the other measurements. It is also lower than most of the other experimental values compiled in [14]. Suzuki *et al.* point out that a similar situation occurred for their measurements of the corresponding oscillator strength in krypton. Although the most recent $f_{\rm res}$ measurements span a wide range, the compiled values indicate a

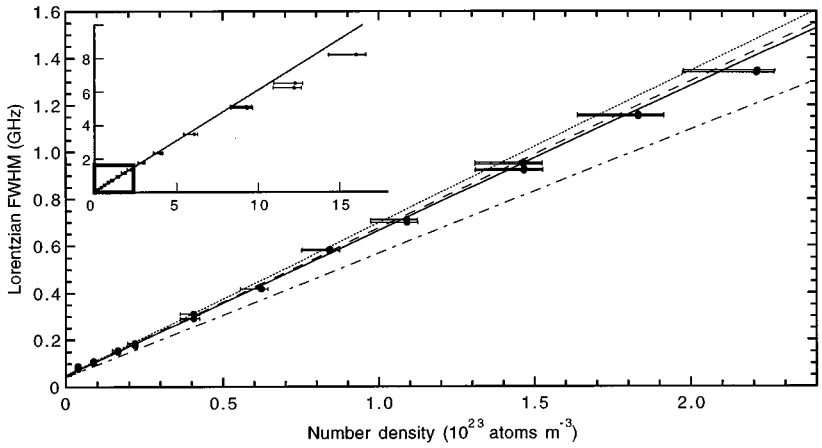

FIG. 5. Plot of $6s[3/2]_1^o \rightarrow 6p[1/2]_0$ $\Delta\nu_L$ versus number density and comparison of measured $\Delta\nu_L$ (•) in the low-density range to impact theory [Eq. (1)] using $\cdots$, $f=0.273$ [14]; ---, $f=0.264$ [40]; -·-, $f=0.222$ [41]; and —, $f=0.260$ [42]. The inset shows the full density range with the expanded region indicated; —, linear fit to low-density points.

consensus around 0.260 [14]. Our data are in remarkable agreement with this value. The agreement of the calculated f_{res} with other measurements demonstrates that the impact approximation resonance broadening theory [Eq. (1)] is equally applicable to heavy inert gases. It also shows that any complications introduced by collisional interactions between different isotopes or with atoms in different hyperfine levels is not substantial.

From Fig. 6(b) it is clear that the Voigt model does not adequately represent the recorded line shapes at the higher densities. These asymmetric profiles make it definite that the nonlinearity of $\Delta\nu_L$ with N of resonance broadened transitions is from the breakdown of the impact approximation. The forced fitting of the Voigt model to the asymmetric high-density line shapes gives an unreliable measure of the FWHM. Thus the nonlinearity of the FWHM with number density in Fig. 5 may be from a combination of a reduction in resonance broadening, as calculated by Srivastava and Zaidi [25] and from the inadequacy of fitting the Voigt model to the asymmetric profile. In any case, the range of validity of Eq. (1) is evident from Fig. 5. The beginning of the nonlinearity defines the breakdown of the impact limit. At the low-density end, measurements become difficult for conditions where the Doppler FWHM becomes much greater than the resonance broadening FWHM. For the conditions of a room-temperature dc discharge, the resonance broadening can be accurately measured roughly from 0.1 to 6 torr.

The impact approximation is often used at significantly higher pressures than encountered in this study for broadening from van der Waals forces. However, the resonance interaction is a longer-range interaction. The validity criterion for the impact approximation $\Delta\nu_L \ll N^{1/3}\overline{v}$ can be used to roughly calculate where the approximation should break down [18]: where $\Delta\nu_L=(2\gamma/N)N\approx(N^{1/3}\overline{v})/10$. Here $\overline{v}$ is

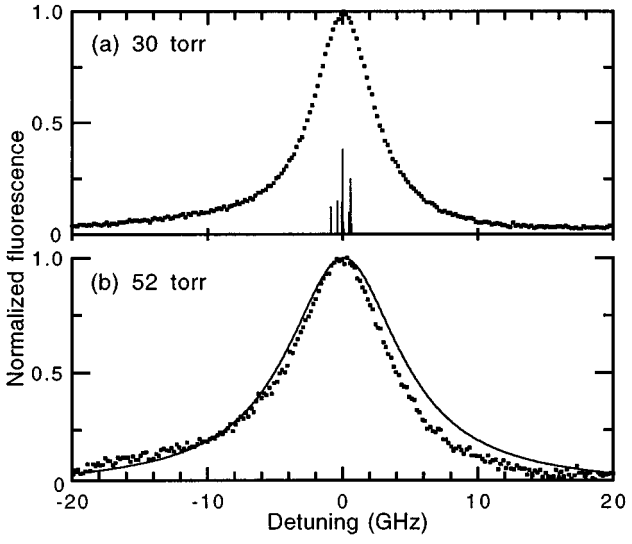

FIG. 6. Asymmetric reduced $6s[3/2]_1^o \rightarrow 6p[1/2]_0$ LIF excitation line shapes (•) at high densities with only every second point plotted for clarity: (a) 9.3×10^{23} atoms m^{-3} with contributing hyperfine lines (|); (b) 1.6×10^{24} atoms m^{-3} with the calculated line shape (—) from the sum of Voigt broadened hyperfine lines using the measured 6.04×10^{-21} MHz m^3 atom^{-1} broadening constant to show the departure from low-density theory; Voigt $a=21$.

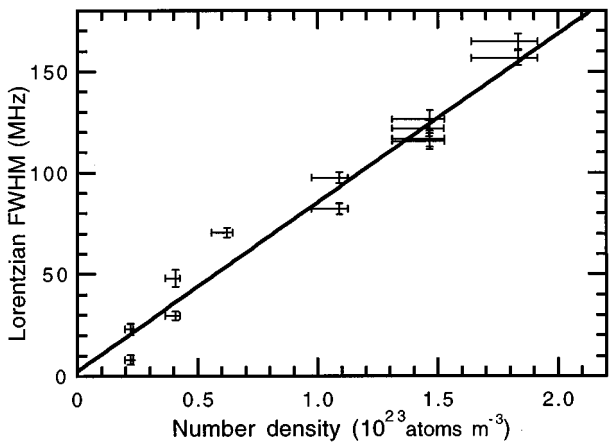

FIG. 7. Plot of $6s[3/2]_2^o \rightarrow 6p[3/2]_2$ $\Delta\nu_L$ versus number density; +, from an analysis of measured line shapes; —, linear fit.

the average relative speed. Using $f_{res}=0.260$ to calculate $2\gamma/N$ from Eq. (1) leads to $N\approx 2\times 10^{23}$ atoms m^{-3} as the estimate for the density at which the impact approximation should begin to break down for the situation considered. This estimate coincides with the beginning of the nonlinearity in our experimental results. The impact approximation also does not apply at frequencies far from line center, even at low densities. However, the portions of the line shapes important to the curve fits do not extend further than a few FWHM's from line center, well within the frequency range of validity except at the highest densities investigated.

As with the previous absorption line-shape measurements [8–10], our data do not show an extrapolation anomaly. The extrapolation of the $6s[3/2]_1^o \rightarrow 6p[1/2]_0$ Lorentzian broadening to zero density should give the natural linewidth plus the laser linewidth. This provides a check of the self-consistency of the measurement of f_{res}. Using our measured $f_{res}=0.255$ value along with a radiative lifetime of the $6p[1/2]_0$ level of 26.8 ns [44] gives 48 MHz for the natural linewidth. This value lies well within the range of uncertainty of our measured 43 ± 15 MHz result.

The average T_{kin} derived from the measured $6s[3/2]_2^o \rightarrow 6p[3/2]_2$ line shapes was a few percent higher than the ambient room temperature. The small amount of discharge heating measured over all discharge conditions is consistent with calculations based on the work of Grimblatov, Mikhailovskaya, and Suniga [45] and with the findings of others [4,9,10]. The T_{kin} extracted from the curve fit was very sensitive to small disagreements in the positions and relative heights of the secondary peaks in the $6s[3/2]_2^o \rightarrow 6p[3/2]_2$ line shape. So, deriving a temperature with an 11% uncertainty is satisfactory considering the complexity of the line shapes. Establishing T_{kin} for the neutral atoms, however, is the main source of uncertainty in our measurements of the resonance broadening.

The Lorentzian component extracted from the $6s[3/2]_2^o \rightarrow 6p[3/2]_2$ curve fit was even more sensitive to slight anomalies in the measured line shapes leading to the large uncertainty in the measurement of the broadening constant. Our $8.3(\pm 1.8)\times 10^{-22}$ MHz m^3 $atom^{-1}$ measurement, though, is in agreement with a previous report of 8.2×10^{-22} MHz m^3 $atom^{-1}$ [46]. As expected, the $6s[3/2]_2^o \rightarrow 6p[3/2]_2$ van der Waals broadening is considerably smaller than the Lorentzian broadening of the $6s[3/2]_1^o \rightarrow 6p[1/2]_0$ transition. This justifies the entire neglect of the dispersion contribution to the $6s[3/2]_1^o \rightarrow 6p[1/2]_0$ line shape. The natural width for the $6s[3/2]_2^o \rightarrow 6p[3/2]_2$ transition is 5 MHz [44]. This value again falls within the uncertainty range of the measured Lorentzian width extrapolated to zero density.

ACKNOWLEDGMENTS

We would like to thank M. D. Di Rosa for his valuable discussions. This work was supported by the United States Air Force Office of Scientific Research, Aerospace Sciences and Materials Directorate.

[1] D. N. Stacey and R. C. Thompson, J. Phys. B **16**, 537 (1983).
[2] J. M. Vaughan, Phys. Rev. **166**, 13 (1968).
[3] J. M. Vaughan, Proc. R. Soc. London Ser. A **295**, 164 (1966).
[4] A. R. Malvern, A. C. Pinder, D. N. Stacey, and R. C. Thompson, Proc. R. Soc. London Ser. A **371**, 259 (1980).
[5] A. R. Malvern, J. L. Nicol, and D. N. Stacey, J. Phys. B **7**, L518 (1974).
[6] A. Atiola, B. C. Gibson-Wilde, A. C. Lindsay, J. L. Nicol, and I. B. Whittingham, J. Phys. B **21**, 249 (1988).
[7] R. Damaschini, A. Malvern, and J. Verges, Phys. Lett. **69A**, 4 (1978).
[8] A. C. Lindsay, J. L. Nicol, D. N. Stacey, and P. E. G. Baird, J. Phys. B **22**, L303 (1989).
[9] A. C. Lindsay, J. L. Nicol, and D. N. Stacey, J. Phys. B **24**, 4901 (1991).
[10] P. E. G. Baird, K. Burnett, R. Damaschini, D. N. Stacey, and R. C. Thompson, J. Phys. B **12**, L143 (1979).
[11] D. N. Stacey and J. M. Vaughan, Phys. Lett. **11**, 105 (1964).
[12] H. G. Kuhn and J. M. Vaughan, Proc. R. Soc. London Ser. A **277**, 297 (1964).
[13] W. R. Hindmarsh and K. A. Thomas, Proc. Phys. Soc. London **77**, 1193 (1961).
[14] W. F. Chan, G. Cooper, X. Guo, G. R. Burton, and C. E. Brion, Phys. Rev. A **46**, 149 (1992).
[15] A. S. Pine, C. J. Glassbrenner, and J. A. Kafalas, IEEE J. Quantum Electron. **9**, 800 (1973).
[16] A. Omont, J. Phys. (Paris) **26**, 26 (1965).
[17] P. R. Berman and W. E. Lamb, Jr., Phys. Rev. **187**, 221 (1969).
[18] H. G. Kuhn and E. L. Lewis, in *Polarisation, Matière et Rayonnement*, edited by La Societé Francaise de Physique (Presses Universitaires de France, Paris, 1969), p. 341.
[19] C. G. Carrington, D. N. Stacey, and J. Cooper, J. Phys. B **6**, 417 (1973).
[20] E. L. Lewis, Proc. Phys. Soc. London **92**, 817 (1967).
[21] D. F. T. Mullamphy, G. Peach, and I. B. Whittingham, J. Phys. B **24**, 3709 (1991).
[22] A. Schwabedissen and W. Bötticher, J. Phys. B **26**, 3467 (1993).
[23] J. Purić, S. Djeniže, J. Labat, A. Srećković, and M. Platiša, Contrib. Plasma Phys. **31**, 63 (1991).
[24] R. Ciurylo, A. Bielski, J. Domyslawska, J. Szudy, and R. S. Trawiński, J. Phys. B **27**, 4181 (1994).
[25] R. P. Srivastava and H. R. Zaidi, Can. J. Phys. **53**, 84 (1975).
[26] S.-Y. Ch'en and M. Takeo, Rev. Mod. Phys. **29**, 20 (1959).
[27] A. O. Vyrodov, J. Heinze, and U. E. Meier, J. Quant. Spectrosc. Radiat. Transfer **53**, 277 (1995).
[28] F. M. Curran, J. S. Sovey, and R. M. Myers, Acta Astron. **29**, 651 (1993).
[29] L. H. Caveny, F. M. Curran, and J. R. Brophy, in *Proceedings of the 23rd International Electric Propulsion Conference, Seattle, 1993* (Ohio State University, Columbus, 1993), Vol. 1, p. 12.
[30] J. G. Liebeskind, R. K. Hanson, and M. A. Cappelli, Appl. Opt. **32**, 6117 (1993).
[31] J. C. Camparo, Contemp. Phys. **26**, 443 (1985).
[32] L. F. Stokes, M. Chodorow, and H. J. Shaw, Opt. Lett. **7**, 288 (1982).

[33] E. Browne *et al.*, in *Table of Isotopes*, 7th ed., edited by C. M. Lederer and V. S. Shirley (Wiley, New York, 1978).
[34] D. A. Jackson and M.-C. Coulombe, Proc. R. Soc. London Ser. A **338**, 277 (1974).
[35] W. Fischer, H. Hühnermann, G. Krömer, and H. J. Schäfer, Z. Phys. **270**, 113 (1974).
[36] D. A. Jackson, F. R. S., and M.-C. Coulombe, Proc. R. Soc. London Ser. A **327**, 137 (1972).
[37] H. Geisen, T. Krümpelmann, D. Neuschäfer, and Ch. Ottinger, Phys. Lett. A **130**, 299 (1988).
[38] H. E. White, *Introduction to Atomic Spectra* (McGraw-Hill, New York, 1934), p. 439.
[39] P. L. Varghese and R. K. Hanson, Appl. Opt. **23**, 2376 (1984).
[40] H. M. Anderson, S. D. Bergeson, D. A. Doughty, and J. E. Lawler, Phys. Rev. A **51**, 211 (1995).
[41] T. Y. Suzuki *et al.*, Phys. Rev. A **43**, 5867 (1991).
[42] W. R. Ferrell, M. G. Payne, and W. R. Garrett, Phys. Rev. A **35**, 5020 (1987).
[43] D. Bessis, A. Haffad, and A. Z. Msezane, Phys. Rev. A **49**, 3366 (1994).
[44] M. R. Bruce, W. B. Layne, C. A. Whitehead, and J. W. Keto, J. Chem. Phys. **92**, 2917 (1990).
[45] V. M. Grimblatov, L. V. Mikhailovskaya, and L. Suniga, Opt. Spektrosk. **77**, 887 (1994) [Opt. Spectrosc. **77**, 797 (1994)].
[46] K. Tachibana, N. Kitagawa, and H. Harima, in *Proceedings of the Third Workshop on Radiation Detectors and Their Uses, Ibaraki, Japan, 1988*, edited by M. Miyajima, S. Sasaki, and T. Doke (National Laboratory for High Energy Physics, Tsukuba, 1988), p. 45.
[47] C. E. Moore, *Atomic Energy Levels*, Natl. Bur. Stand. (U.S.) Circ. No. 467 (U.S. GPO, Washington, DC, 1958), Vol. III, p. 113.